Interference of tectonic signals in subsurface hydrologic monitoring through gravity and GPS due to mountain building

Wenjin Chen, Carla Braitenberg, Enrico Serpelloni

PII: S0921-8181(17)30578-7
DOI: doi:10.1016/j.gloplacha.2018.05.003
Reference: GLOBAL 2771

To appear in: *Global and Planetary Change*

Received date: 10 November 2017
Revised date: 1 May 2018
Accepted date: 17 May 2018

Please cite this article as: Wenjin Chen, Carla Braitenberg, Enrico Serpelloni , Interference of tectonic signals in subsurface hydrologic monitoring through gravity and GPS due to mountain building. The address for the corresponding author was captured as affiliation for all authors. Please check if appropriate. Global(2017), doi:10.1016/j.gloplacha.2018.05.003

Interference of tectonic signals in subsurface hydrologic monitoring through gravity and GPS due to mountain building

, Wenjin Chen[1,2,3], Carla Braitenberg[3], Enrico Serpelloni[4]

[1] School of Geomatics Science and Technology, Nanjing Tech University, Nanjing, P.R. of China.

[2]School of Geodesy and Geomatics, Wuhan University, P.R. of China

[3]Department of Mathematics and Geosciences, University of Trieste, Italy

[4]INGV

Corresponding author: Prof. Carla Braitenberg

Postal address: Department of Mathematics and Geosciences, University of Trieste, Trieste 34127, Via Weiss 1, Italy (Email: berg@units.it)

Abstract: Global Positioning System observations in the Alps have now sufficient precision to reliably observe vertical surface movement rates at the orogen scale. The geodynamic modeling of converging plate margins requires constraints on the origin of orogenic uplift, of which the two end members are pure crustal uplift and crustal thickening, respectively. Gravity change rates joint with uplift measurements allows to distinguish the two mechanisms. We use vertical uplift rates over the Alpine range and the southern foreland basin, to predict the gravity change for different geodynamic hypotheses of pure uplift and mantle inflow, or crustal thickening and isostatic Moho lowering. The sensitivity of gravity as a tool to distinguish the two mechanisms is investigated. This model differs from the predicted isostatic movements, based on the glacial history and the mantle viscosity, since the uplift is measured and not predicted. The estimate of this tectonic signal is important, when gravity change rates, as those obtained from GRACE, are interpreted exclusively in terms of hydrologic changes tied to climatic variation. It has been already shown that in some areas, as the Tibetan plateau and the Himalayas, the tectonic signal is not negligible. Here we estimate the effect of the tectonic signal for the uplift of smaller mountain ranges, as is the Alpine arc. Our results indicate that tectonic and hydrological signals superpose and we cannot ignore the tectonic signal when using GRACE to invert for the equivalent water height (EWH).

Keywords: tectonic signals, GPS, satellite gravity model, Alpine arc

1. Introduction

The Alps are the highest and the most extensive mountain range system that lies entirely in Europe, crossing eight countries: Italy, Austria, France, Germany, Slovenia, Monaco, Liechtenstein and Switzerland (see Fig.1) The Alpine orogen results from the collision of the European and Adriatic plates after subduction of intervening ocean basins (e.g., Dewey et al., 1973; Molnar and England, 1990; Pfiffner, 2014). The collision took place in the Tertiary but was preceded by other collision events in the Cretaceous (Gerrard, 1990). The Alpine orogeny was very complex and occurred in several phases from the middle Cretaceous to the Neogene, of which the collision between Europe and Africa was only one. Global Positioning System (GPS) data and earthquake focal mechanisms show that the Adria-Eurasia convergence is still active in the Eastern Alps (Serpelloni et al. 2016), whereas it is ceased in the western Alps, where seismotectonic and geodetic data indicate small extension across the belt. On the contrary, **GPS** vertical rates (e.g., Serpelloni et al., 2013) show that large part of the Alpine range is uplifting and a number of researchers put forward various mechanisms to explain this phenomenon. Several works concentrate on the Western Alps, such as Chéry et al. (2016) who investigated the rheological model in the western Alps and concluded that a significant part of the geodetic uplift may represent the coda of a postglacial rebound occurring during the Holocene. Nocquet et al. (2016) combined continuous **GPS** with leveling data spanning a century to study the present-day vertical motion in the western Alps and its surroundings. They thought that rock-uplift rates corrected for transient glacial isostatic adjustment (GIA)

contributions likely exceed erosion rates in the northwestern Alps and in the absence of active convergence, the observed surface uplift must result from deep-seated processes. Vernant et al. (2013) showed that in the western Alps low converge rates are measured, and concluded that the erosional processes are the predominant control on the present-day deformation and seismicity. Champagnac et al. (2007, 2009) proposed that the erosion of the Western Alps could explain part of the modern vertical motions through isostatic rebound. A further mechanism has been proposed to be due to lithospheric slab displacement that can disturb the isostatic equilibrium and result in vertical movement (Lyon-Caen et al., 1989; Singer et al., 2014; Fox et al., 2015).

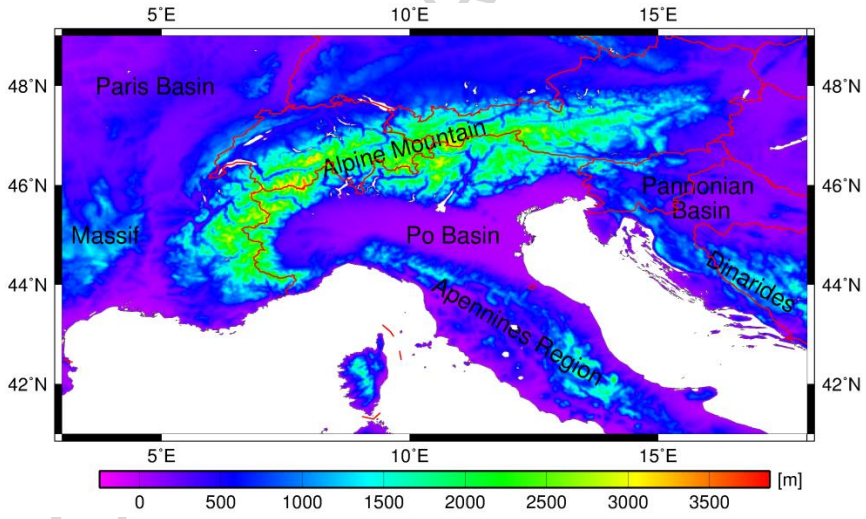

Fig.1 Topography of studied area covering the Alpine arc (ETOPO1, Amante and Eakins, 2009)

Topography uplift leads to mass redistribution, both at the earth surface and inside the earth, and as a result creates gravity changes. In this study we intend to model the mass changes that can be expected by topography uplift and for different assumptions on the deep processes accompanying the topography uplift.

Mass redistribution can be detected in changes of Earth's gravity field observed either on ground or by satellites, for instance by the Gravity Recovery and Climate Experiment (GRACE) (Tapley et al., 2004a, 2004b). The GRACE mission records changes in Earth's gravity field at spatial resolution of about 300 km and temporal resolution of one month, since 2002. On the other hand, ESA's Gravity field and steady-state Ocean Circulation Explore or GOCE mission (Floberghagen et al., 2011) has better spatial resolution than GRACE (about 80 km resolution) but a much shorter life time of about 5 years (2009-2013), which limits its ability to detect the climatic or geodynamics changes (Pail et al., 2015a; 2015b). The static field of GOCE (Pail et al., 2011) has been shown to allow to identify geological structures and lineaments in different areas of the world (e.g. Alvarez et al., 2014; 2015a; Braitenberg, 2014; 2015; Li et al., 2017; Shin et al., 2015) and the time variable part has been shown to match expected changes generated by mega-earthquakes along the Andean subduction margin (Alvarez et al., 2015b). The GOCE field has been also shown to be useful in the control of terrestrial data of higher spatial resolution than the GOCE minimum wavelength (Bomfim et al., 2013).

Therefore, in this study we use a GRACE-GOCE satellite combined Earth's gravity model GOCO05S (Mayer-Guerr and GOCO team, 2015) to compute the observed gravity change signal and compare it with our prediction results. The contents of this manuscript are organized as follows. We first present the data, which include a decade of **GPS** vertical rates, ETOPO1 topography (Amante and Eakins, 2009), CRUST1.0 Moho depth (Laske et al, 2013), GOCO05S Earth's gravity model,

groundwater levels data and the GLDAS-1 Noah model (monthly and 0.25 degree resolution). Then we briefly introduce the methodology, which aims at matching the observed vertical rates and hydrologic data with the observed gravity changes. For this purpose, we consider different mechanisms (Cloetingh and Ziegler, 2009; Cloetingh and Burov, 2011; Braitenberg and Shum, 2017) to model the mass changes at the crust-mantle interface, which accompany the topography uplift. We then model the expected gravity signal due to the hydrologic component based on observations, using both the measured underground water level data and the soil moisture models. Finally, the modeled data are compared with the GOCO05S observation signal of gravity change in time.

2. Methodology

2.1 Modeling the gravity change due to topographic uplift and crustal response

We use two end-member mechanisms to model the tectonic signal. The two end-members represent the maximum and minimum mass change at Moho level that can be expected accompanying orogenic topographic vertical movements. The first model assumes that topography and Moho interface uplift at the same rate (see Braitenberg and Shum, 2017), implying mantle flow replacing the crust at the same rate. The second model assumes that topography uplift is isostatically compensated by crustal thickening implying Moho lowering at the rate defined by Airy's hypothesis. The reason to use the Airy model and not a flexural model is due to the fact that the greatest expected Moho lowering for the flexural model is obtained with

zero flexural rigidity, which corresponds to the Airy response.

According to Airy's model, for a topography uplift rate of $T\ mm/yr$, the corresponding Moho lowering rate is defined by

$$\Delta h = \frac{\rho_c}{\rho_m - \rho_c} T \quad (1)$$

Where ρ_m and ρ_c are the density of mantle and crust, respectively. Computation of the topographic and Moho gravity changes are done by first discretizing the static topography and the starting Moho depth (see Fig.2) by prisms (Uieda et al., 2016). The mass change due to topography or Moho movement is again discretized as prisms and added to the static prism model. The gravity change is obtained from subtracting the static model from the dynamic model.

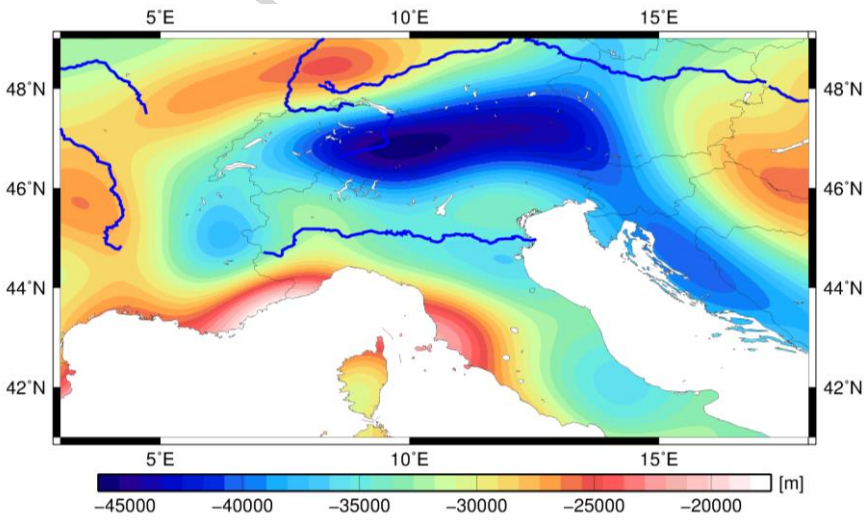

Fig.2 Moho depth (from CRUST1.0 model, Laske et al., 2013)

The height of the calculation is 10km, in order to be above all elevations. The

adopted crust density value is 2670 kg/m^3 (Hinze, 2003) and the mantle density value is 3200 kg/m^3 (Lippitsch et al., 2003; Levandowski et al, 2014). In case of the topographic uplift we assumed positive crustal density contrast with respect to air while for Moho uplift we used the density contrast between mantle and crust. The positive mass change in case of Moho uplift physically is due to the influx of mantle replacing the space of the uplifting crust. The process is assumed to be slow enough that viscosity effects of the mantle do not significantly introduce a time shift between topography uplift and the mantle influx. The mantle movement towards the area in which Moho depth is changing contributes to a density change only where mantle replaces crust, with a considerable density contrast. The density changes in the mantle are assumed sufficiently homogeneous to not contribute significantly to the calculations, as their variation is much smaller than the density contrast between crust and mantle. The Moho uplift model would represent the topographic uplift controlled by dynamic, mantle-driven processes, that have been suggested to occur at plate margins (e.g., Faccenna et al. 2014). The Moho lowering model would describe a situation in which crustal thickening occurs, due to horizontal compression.

2.2 Gravity change rate from GOCO05S

We use the spherical harmonic synthesis (SHS) to compute the gravity changes observed from the GOCO05S model (Mayer-Guerr and GOCO team, 2015). The gravity changes δg reads

$$\delta g = \frac{GM}{R^2} \sum_{n=0}^{\bar{n}} \sum_{m=-n}^{n} \left(\frac{R}{r} \right)^{n+2} (n+1)\, T_{n,m}\, Y_{n,m}(\Omega) \tag{2}$$

where $GM = 3986005 \times 10^8$ m^3/s^2 is the geocentric gravitational constant, $R = 6371 \times 10^3$ m is the Earth's mean radius (which approximates the geocentric radius of the geoid surface), $Y_{n,m}$ are the surface spherical harmonic functions of degree n and order m, $T_{n,m}$ are the linear trend coefficients, and $\bar{n}$ is the maximum degree of spherical harmonics, where for the GOCO05S model the value is 100. The GOCO05S trend coefficients were calculated integrating the GOCE observations with GRACE (metadata published together with the model). The 3-D position is defined in the system of geocentric spherical coordinates (r, Ω), where r is the geocentric radius, and $\Omega = (\varphi, \lambda)$ denotes the geocentric direction with the spherical latitude φ and longitude λ.

2.3 Gravity effect of hydrology

The computation of the hydrologic gravity effect implies knowledge on the mass change due to hydrology. The direct observation limits to groundwater data from monitored wells. The soil moisture is an indirect measure that is available globally and that has a lower spatial resolution than the wells data. For both datasets we must determine the average linear rate change, which we determine together with a yearly oscillation. We use the following model to fit the data, where for each station the time series $f(\theta, \lambda, t_i)$ (i=1, 2… n. n is the number observations) has the following mathematical expression,

$$f(\theta, \lambda, t_i) = a_0 + a_1 t_i + a_2 \cos \omega t_i + a_3 \sin \omega t_i + noise \quad i = 1, 2..., n \tag{3}$$

where a_0 is the starting value at the time of origin,

a_1 is the linear trend,

a_2 is the annual cosine component,

a_3 is the annual sine component,

ω is the circular frequency with yearly period

Eq.(3) can be rewritten as

$$\begin{bmatrix} 1 & t_1 & \cos\omega t_1 & \sin\omega t_1 \\ 1 & t_2 & \cos\omega t_2 & \sin\omega t_2 \\ \dots & \dots & \dots & \dots \\ 1 & t_n & \cos\omega t_n & \sin\omega t_n \end{bmatrix} \begin{bmatrix} a_0 \\ a_1 \\ a_2 \\ a_3 \end{bmatrix} + noise = \begin{bmatrix} f(\theta,\lambda,t_1) \\ f(\theta,\lambda,t_2) \\ \dots \\ f(\theta,\lambda,t_n) \end{bmatrix} \tag{4}$$

Defining the design matrix as $\mathbf{A}$, solution vector as $\mathbf{X}$ and the observation vector as $\mathbf{Y}$, where

$$\mathbf{A} = \begin{bmatrix} 1 & t_1 & \cos\omega t_1 & \sin\omega t_1 \\ 1 & t_2 & \cos\omega t_2 & \sin\omega t_2 \\ \dots & \dots & \dots & \dots \\ 1 & t_n & \cos\omega t_n & \sin\omega t_n \end{bmatrix}, \quad \mathbf{X} = \begin{bmatrix} a_0 \\ a_1 \\ a_2 \\ a_3 \end{bmatrix} \quad \text{and} \quad \mathbf{Y} = \begin{bmatrix} f(\theta,\lambda,t_1) \\ f(\theta,\lambda,t_2) \\ \dots \\ f(\theta,\lambda,t_n) \end{bmatrix} \tag{5}$$

Based on the least square rule, the solution for $\mathbf{X}$ reads

$$\mathbf{X} = (\mathbf{A}^{\mathrm{T}}\mathbf{A})^{-1}\mathbf{A}^{\mathrm{T}}\mathbf{Y} \tag{6}$$

The solution vector **X** will be space dependent and describes the local linear trend and phase and amplitude of the yearly variation for each hydrologic station. The stations are only available in the flat basin, and are unavailable when topographic elevation increases. We therefore refer to the global soil moisture model, which represents modelled variation of soil moisture in the first 2m of soil. The gravity change rate of

the soil moisture is obtained in spherical harmonics, concatenating the spherical harmonic analysis (SHA) and spherical harmonic synthesis (SHS) method to compute the gravity change. The SHA (Chao and Gross, 1987; Wahr et al, 1998) is defined as:

$$\begin{Bmatrix} \Delta C_{nm} \\ \Delta S_{nm} \end{Bmatrix} = \frac{3}{4\pi R \rho_{\text{ave}}(2n+1)} \int_0^{2\pi} d\phi \int_0^{\pi} \sin\theta d\theta \times \Delta\sigma(\theta,\lambda) \overline{P}_{nm}(\cos\theta) \begin{Bmatrix} \cos m\phi \\ \sin m\phi \end{Bmatrix} \quad (7)$$

Where in this study $\Delta\sigma(\theta,\lambda)$ stands for linear trend of soil moisture, ρ_{ave} is the average density of the earth ($5500\,kg/m^3$), $\overline{P}_{nm}(\cos\theta)$ is the normalized Associate Legendre Function (ALF). Finally, we combined equations (7) and (2) to compute the gravity change. According to the rule of thumb of SHA, we expand the soil moisture linear trend to degree/order 720 and limit the further analysis to degree 100, for the comparison with GOCO05S.

3. Data

3.1 Vertical rates from GPS and Moho model

GPS vertical ground motion rates are updated from Serpelloni et al. (2013), using data up to the end of 2016, with a minimum of 2.5 and a maximum of 23 years, for a limited number of sites, from more than 800 continuous **GPS** stations operating in the study area (Fig. 1). The average time-span of **GPS** sites is 7.5 years. We refer to Serpelloni et al (2013 and 2016) for details on the GPS data analysis.

The GPS velocities are realized in the IGb08 reference frame (Rebischung et al., 2011), which is the GPS realization of the ITRF08 reference frame (Altamimi et al.

2011). The coordinate origin of the ITRF08 is theoretically defined as the mean center of mass of the total Earth system about which all Earth satellites orbit. Following Wu et al. (2011), the ITRF2008 origin realization is consistent with the mean center of mass at a level of 0.5 mm yr−1, in agreement with the results of Altamimi et al. (2011).

The position of the gravity satellite GOCE and GRACE are precisely determined by **GPS** (e.g. Bock et al., 2011), and are also referenced to the Earth center of mass. Therefore the systems in which gravity rates are observed and rates are predicted from topographic uplift, are consistent.

The rates of vertical land motion are shown in Fig.3, where the single station rates have been interpolated with adjustable tension continuous curvature splines, giving the minimum curvature solution (GMT tool surface, with tension 0.75, Smith and Wessel, 1990). Single **GPS** values and the smoothed vertical velocity field indicate that the Alpine range is overall characterized by positive vertical rates, with maximum values up to 2.5 mm/yr in the western and central Alps. The Po basin in contrast is subsiding with the maximum rate of -7 mm/yr. In the Pannonian basin and surrounding units we can observe uplift as well as subsidence, with possibly larger negative rates compared to the positive rate. The Paris basin is characterized by a prevailing subsidence with some parts having slower vertical motion than the general trend. In the Apennines, even though some stations are subsiding, most of the central part is uplifting, accordingly to Faccenna et al (2014). We use the **GPS** vertical rates to compute the gravity changes due to topography uplift and the corresponding Moho

uplift and lowering, according to the two extreme models.

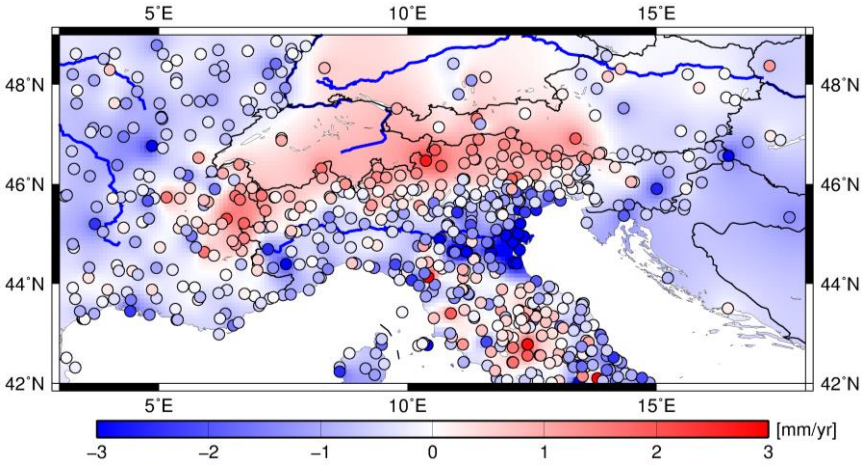

Fig.3 Rates of vertical land motions from **GPS** time series. Updated from Serpelloni et al., 2013.

ETOPO1 (Amante and Eakins, 2009) is a 1 arc-minute global relief model of Earth's surface that integrates land topography and ocean bathymetry. It is compiled from various global and regional datasets such as SRTM30 global topography, Baltic Sea bathymetry, Antarctica RAMP topography, Greenland NSIDC bedrock, GSHHS (Global Self-consistent, Hierarchical, High-resolution Shoreline). The Alpine and surrounding mountain regions (see Fig.1) have the maximum topography to about 4000m while the main elevation of the Pannonian basin, Po basin and Paris basin is just about 450 m above sea level.

The gravity effect due to mass changes at Moho level are calculated imposing the depth variations to a published Moho model. We refer to the model CRUST1.0 (Laske et al., 2013) with 1×1 arc-deg spatial resolution. This model was prepared and administered by the U.S. Geological Survey and the Institute for Geophysics and Planetary Physics at the University of California. The CRUST1.0 consists of the ice,

water, (upper, middle and lower) sediments and (upper, middle and lower) crustal layers. The lower crustal layer is the Moho depth that we adopted in this study. When we compare the topography and Moho depth of the CRUST1.0 model (Fig.2) we can see clearly the spatial anti-correlation between the topography and the Moho depth with the maximum Moho deepening under the highest mountains, indicating that there is isostatic compensation. This has been shown previously in several studies such as Ebbing (2004) and Braitenberg et al. (1997) .

3.2 Hydrologic data groundwater and GLDAS

We use two datasets to estimate the hydrologic contribution to the gravity field. The first is the direct water table observation in wells, which is available for the Po basin and the Venetian plain, but not for the surrounding mountain ranges. In Italy the Environmental Protection Agencies of Piedmont, Lombardy, Veneto and Emilia Romagna and the Friuli Venezia Giulia Region collect groundwater water level data of the Po basin and neighboring basins, and the data have been made available for the present study. We select the stations that have at least 8 years of observations time span for our analysis, so that the yearly variation does not affect the calculated trend.

The Global Land Data Assimilation System (GLDAS) (Rodell et al., 2004), currently has four land surface models: Mosaic, Noah, the Community Land Model (CLM), and the Variable Infiltration Capacity (VIC). The hydrological data used in this study is from the GLDAS-1 Noah model. GLDAS provides the 3-hourly or monthly 0.25 and 1.0 degree products globally. In this study, the monthly 0.25 degree resolution products are employed. In the Noah model, there are four layers of soil

moisture that we integrate by summing up the four layers, obtaining a time-series from January 2003 to December 2013. Then a temporal model consisting of constant, linear and annually varying terms are fitted to the soil moisture time series at a regular grid as defined in Eq.(6). Finally, we obtain the spatially varying linear trend of the soil moisture from GLDAS-1 Noah model.

3.3 Observed gravity changes from satellite

The model GOCO05S (Mayer-Guerr and GOCO team, 2015) can provide us the gravity changes per year from linear spherical harmonic coefficients up to degree/order 100. GOCO05S was obtained from processing the data from GRACE: ITSG-Grace2014s (2003-2013), GOCE (2009-2013), kinematic orbits (Swarm A+B+C, TerraSarX, CHAMP, GRACE A+B, GOCE) and SLR (LAGEOS). The GOCO05S spherical harmonic coefficients consist of static (N= 280, corresponding to spatial resolution of about 70km), linear trend (N=100, ibid, about 200km), which is centered on year 2008, and yearly oscillation (N=100, ibid). As the GOCO05S gravity model combines information from GRACE and GOCE, the spatial resolution of its static part spatial can reach about 70 km, due to the use of all data from the GOCE mission; whereas its linear trend and yearly oscillation can achieve the resolution of 200km, which is higher than the GRACE 300km spatial resolution. Therefore the combined GOCE-GRACE linear variation of the gravity field over the limited life-span of GOCE has the greatest spatial resolution presently available, which is important given the relatively reduced size of the Alpine orogen, compared to the Himalaya, Tibet or Andes mountain ranges. Consequently the price for achieving a

better spatial resolution to detect the climatic or geodynamic changes is at a price of reduced time span of the observed gravity change used for the linear interpolation of the gravity change rate.

4. Results and Discussion

4.1 Description of the observed gravity change rate

The GOCO05S (Mayer-Guerr and GOCO team, 2015) observed gravity change rate is shown in Fig.4. As seen from western to eastern Alps the gravity changes from negative to positive rates. In the Apennines region the gravity has a prevailing positive rate with maximum values up to about 0.6 10^{-3} mGal/yr. In the western sector of the Po basin the gravity signal is negative, while moving to the east it gradually increases toward positive values. In the western Pannonian basin at the foot of the Dinarides and over the Dinarides the gravity trend shows maximum negative signal, which accounts to about -0.6 10^{-3} mGal/yr. The northern Pannonian basin has a positive trend. In the north-western part of the figure corresponding to the Paris basin, we observe positive signal while the negative trend is seen southward, roughly corresponding to the Massif Central region. Along the Alpine mountain range, the spatial correlation between observed gravity change rate and topography is poor.

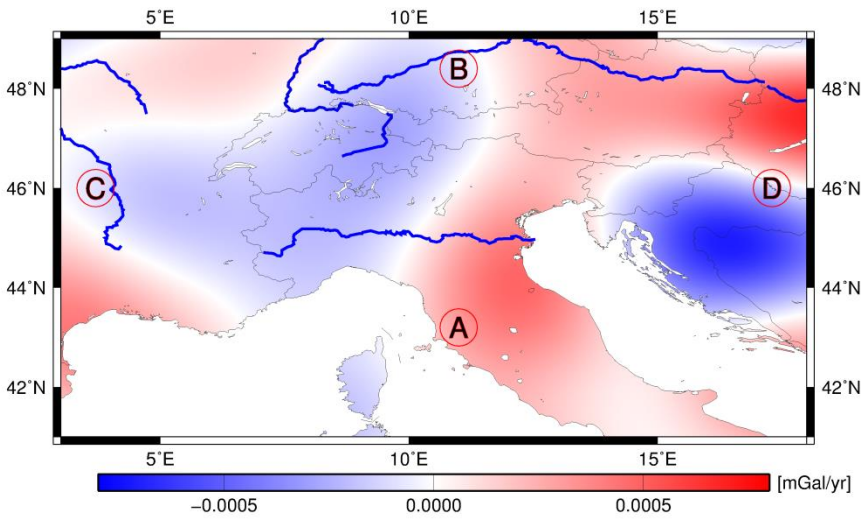

Fig.4 GOCO05S observed gravity change rate (A-B and C-D are the endpoints of the North-South and East-West profiles shown in Figure 10a,b, respectively.).

4.2 Gravity change rate due to topography and Moho vertical movement

The gravitational effect of topographic uplift (see Fig.5a) in the Alpine range reaches maxima up to about 0.2 10^{-3} mGal/yr. Over most of the Paris basin, Po basin and Pannonian basin region, it shows negative values while over the Apennines it gives positive ones. The spatial distribution of the gravitational effect of Moho uplift (see Fig.5b) is similar to the topographic effect but it is much smoother, as being the Moho deeper it acts as a low-pass filter. The Moho uplift signal in the Alps is positive, because as the Moho uplifts then the underlying mantle flows to fill the space, contributing to a positive gravity effect. In the other end-member model, with Moho lowering due to crustal thickening, the lower crust pushes the underlying mantle away, leading to a mass deficit that produces a negative gravity effect, as can be seen over the Alpine range (see Fig.5c)

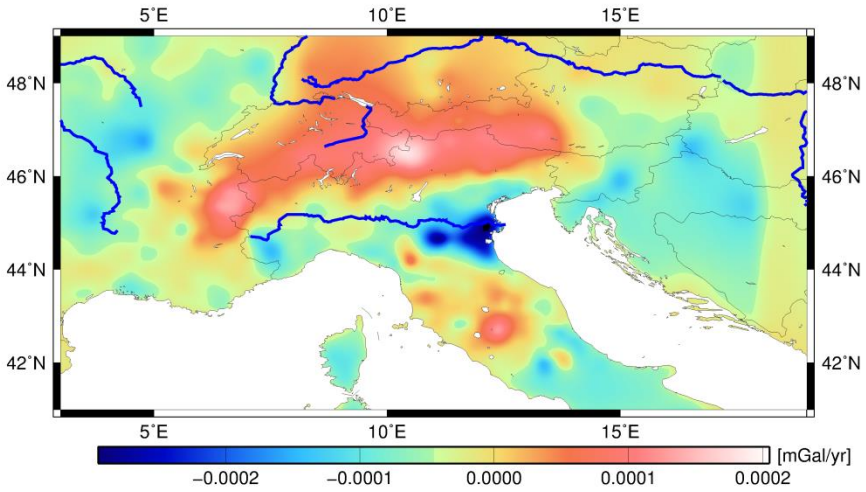

a

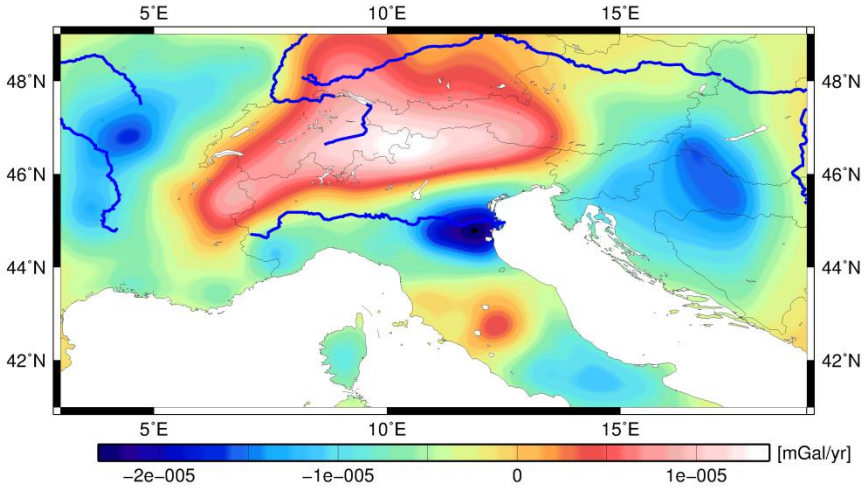

b

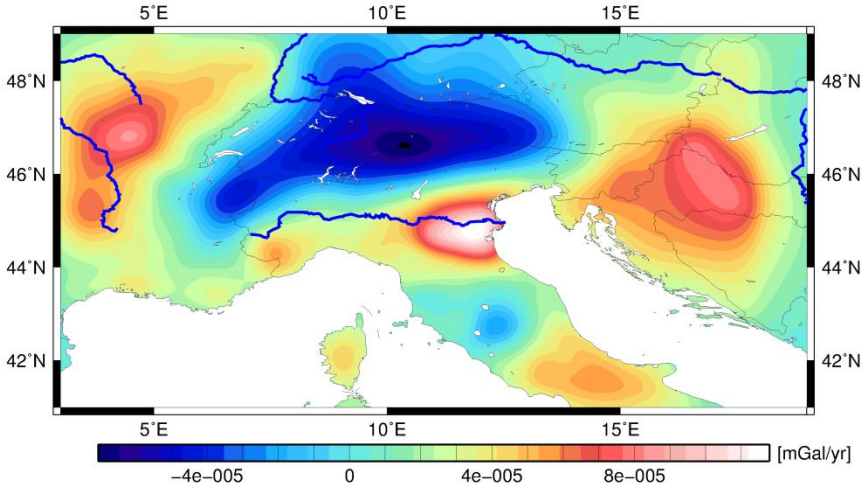

c

Fig.5 (a) Gravity effect due to observed topographic uplift; (b) Gravity effect of Moho uplift with same rate as topography; (c) Gravity effect of crustal thickening and consequent isostatic Moho lowering.

We computed the combined topographic uplift and the corresponding Moho uplift (named Model I) gravity effect (see Fig.6a) and the combined topography uplift and the corresponding Moho lowering (named Model II) gravity effect (see Fig.7a). Model I and Model II revealed that in the Alps the gravity signal can reach about 0.1~0.3 10^{-3} mGal/yr, which contributes to about 25%~30% of the observed signal. Generally, the crustal thickening model (Model II) gives a smaller signal than the topographic uplift model, reducing the gravity effect to 50%. Comparison of the two models shows that in the Alps region, the gravity signal of Model II is much narrower than Model I, since the Moho lowering compensates some topography uplift gravity signal. For the Pannonian basin, Model I has a negative trend while Model II has a subdued signal, comprising positive and negative signals. Model I gave us much more negative signal for the Paris basin, while Model II shows on average subdued negative signal. In the Po basin both models together show negative gravity rate, and both have positive rate for the Apennines.

4.3 Comparison of observed and modeled gravity change rates

When we compare the gravity rates of the two models with the observed gravity signal we can see that in the Pannonian basin Model I agrees well with the observation, except that the amplitude of the modelled signal is too small and

reproduces only about 20% of the amplitude; Model II gives a weak signal close to zero, with some small negative values. In the eastern part of the Alps both models closely agree with observation, predicting positive rates; Model I shows higher amplitude than Model II because Model I enhances the topographic uplift gravity signal by Moho uplift, while Model II compensates part of the signal with Moho lowering. As the observation gravity signal is calculated with spherical harmonic coefficients up to degree/order 100, in order to make a consistent comparison we applied a 500km Gaussian filter to both Models I and II. The results are shown in Figs.6b and Fig.7b, and it is seen that the filtering reduces the maximum amplitudes of the modelled gravity rate, since it smooths the variations. When we compare the filtered results with the observed change rate, we find that the modelled signal can contribute with up to 10% to the observations, and that the relative contribution is stronger where the topographic vertical movement is strongest, and the observed gravity change rate is low. An example is given by the Po basin, where due to the strong subsidence the contribution of the topography could be as large as $-0.04\ 10^{-3}$ mGal/yr, against an observed rate of $0.3\ 10^{-3}$ mGal/yr. We see that the observed signal has greater amplitude than the signal expected through the vertical movements, and only partially correlates with the predicted gravity signal, so it is masking the uplift/subsidence signal due to a further mass change.

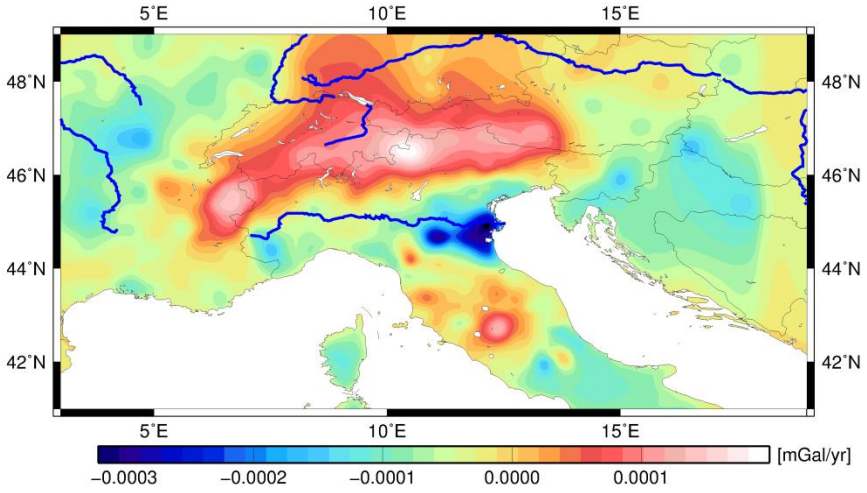

a

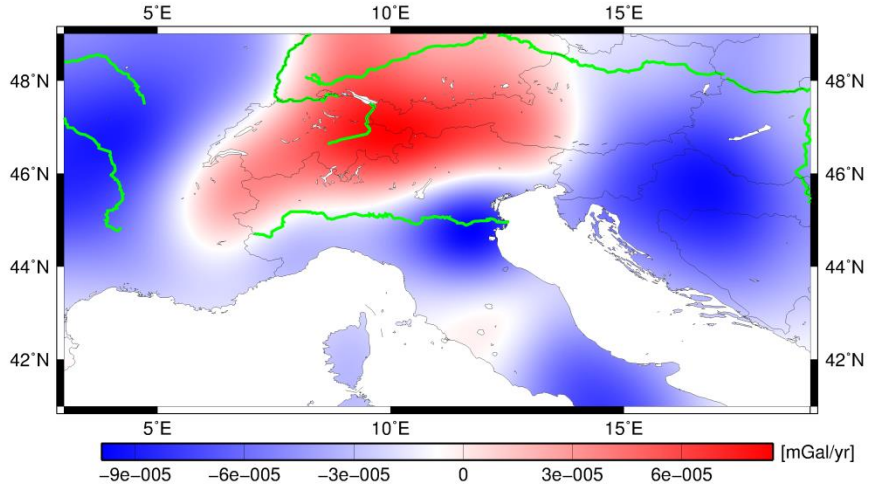

b

Fig.6 (a) Combined topographic uplift and the corresponding Moho uplift gravity effect; **(b)** filtered with 500km Gaussian filter.

In the Po basin it could be argued that the subsidence is due to compaction of sediments, which would reduce the amplitude of the mass change, and would depend on the initial porosity and its evolution in time. If instead the subsidence is due to extraction of water in the deeper layers, with consequent water release from the clay acquitard, being the lowest sealing layer (Martinelli et al., 2014), the subsidence would be due to a mass loss of water, and not rock of a similar volume.

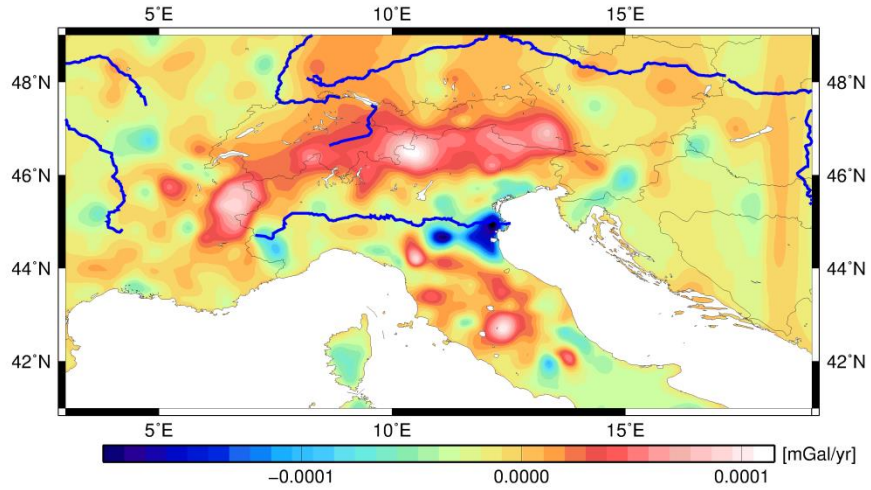

a

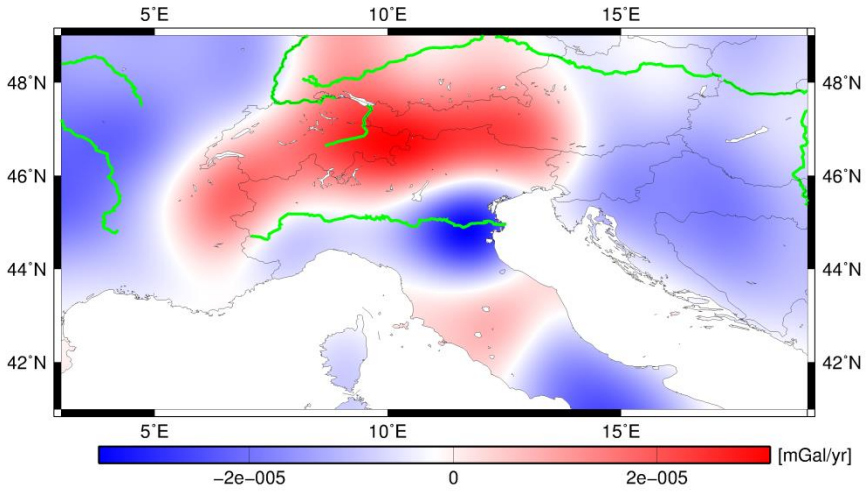

b

Fig.7 (a) Combined topographic uplift and the corresponding Moho lowering gravity effect; **(b)** filtered with 500km Gaussian filter.

In the Alpine range the observed uplift cannot be put away as non-existing, since it is well measured by **GPS**, and the uplift is consistent over the entire mountain range. Presently it is masked by the other mass changes, presumably atmosphere and hydrologic effects, but the models we have calculated show that a better understanding of the non-tectonic mass changes will allow to isolate the tectonic gravity signal and draw conclusions on the crustal compensation mechanism, since it

affects both the geometry of the gravity rate and the amplitude.

4.4 Estimated gravity change rates due to hydrology

In order to verify whether the observed rates agree with the hydrologic signal, we calculate the expected change of the Po basin with the hydrologic data and for the entire region using the GLDAS-1 Noah model moisture product. The observed water levels are available in the lowlands, and are densely distributed (see Fig. 8a). Trends calculated over periods comparable with those from other data reach peaks of 1.5 m/yr, with most values being confined to a trend of 0.3 m/yr. Converting this trend into water mass overestimates the expected signal, because the porosity is not accounted for. But the porosity is not available and the groundwater is in very different environs, ranging from sand to gravel, so a more realistic estimate is not feasible. What the predictions do show is the sign and pattern of the expected gravity variation, and the maximum possible amplitude. The gravity change is negative at the foot of the Apennines, and moderately positive at the northern and southern border of the Po basin (see Fig. 8b). Gravity rates are very strong and reach 20 10^{-3} mGal/year. This value would correspond to a water-mass completely filling the volume of the changing water level, but can be reduced by a factor 10 or 100 when considering presence of sand or gravel, leading to rates in the order of 2 10^{-3} mGal/year or 0.2 10^{-3} mGal/year.

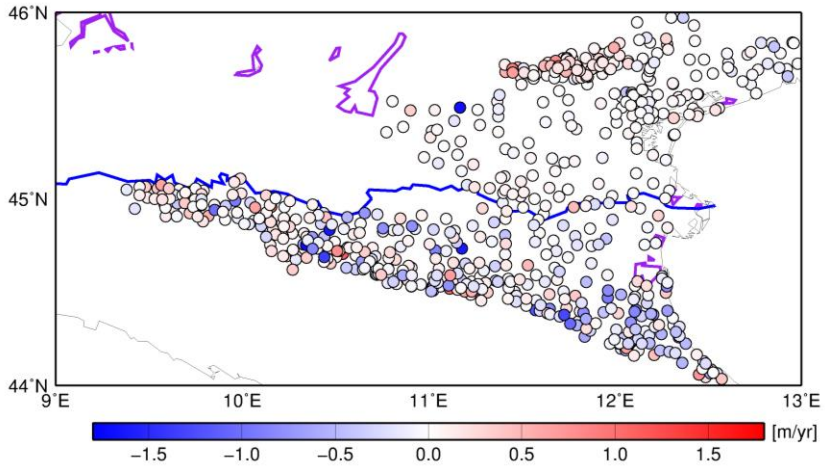

a

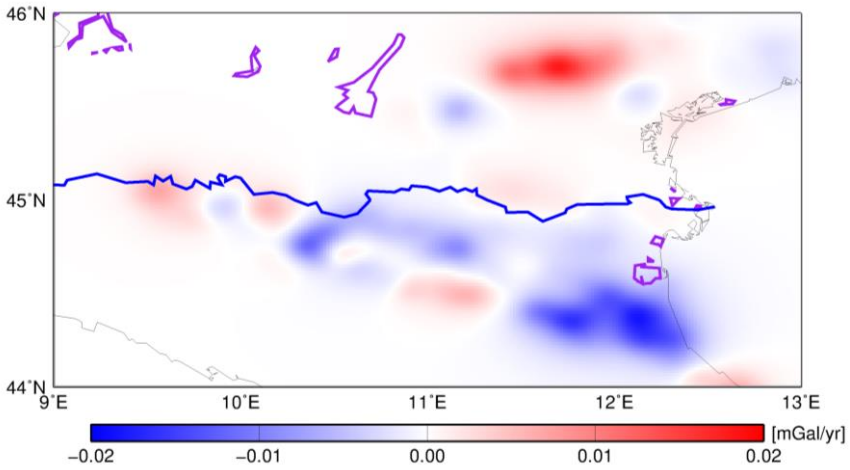

b

Fig.8 (a) Observed Ground water average change rate from direct piezometric observations; **(b)** the corresponding modelled gravity change rate.

The GLDAS-1 Noah model (see Fig.9a) is consistent with the local piezometers of the Po basin, showing a drawdown of water level at the foot of the Apennines, and an increase of level at the southern and northern border of the basin. At larger scales, it is seen that the entire border of the Alps shows an increase of water level, with lower slightly positive values over the range. Paris basin shows a positive increase rate, the Pannonian basin shows a negative rate, disturbed by local positive

increments. Calculating the gravity change rate for the moisture model leads to values up to 1 10^{-3} mGal/year (see Fig. 9b). To be comparable with the observed gravity rate, we apply again the low pass filter, which eliminates all detailed variations, reducing the amplitude to a value of 0.4 10^{-3} mGal/yr and shows only broad patterns (see Fig.9c). The entire Italian territory south of the river Po has a small negative rate, the Alpine range and Paris basin have a positive rate, and the western Pannonian basin has negative rate. Comparison to the observed rates (see Fig.4) reveals several inconsistencies, in particular over the Po basin and Apennines, over the Alpine range and west of it, in the French territory. The Pannonian basin matches the observations, characterized by a negative gravity rate. The order of magnitude of the observed and hydrologic signal is similar, but the pattern is only partially consistent, implying that a further mass variation must exist that generates the observed gravity change.

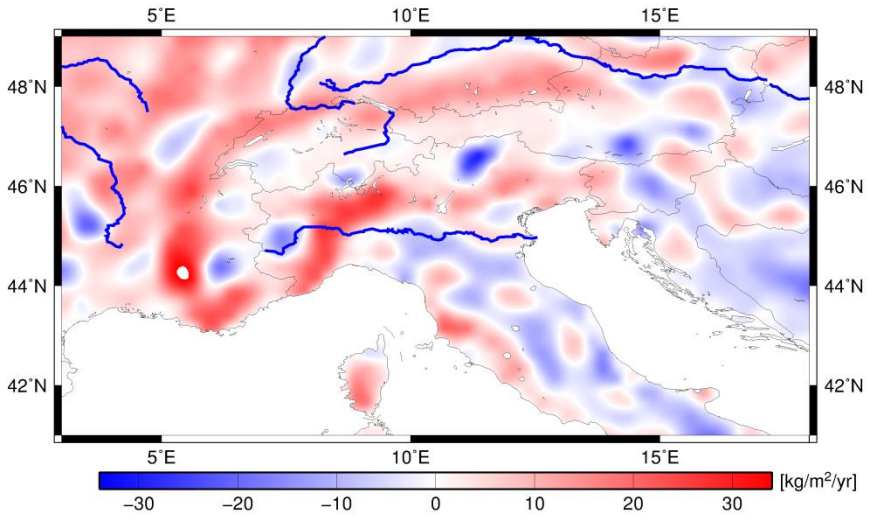

a

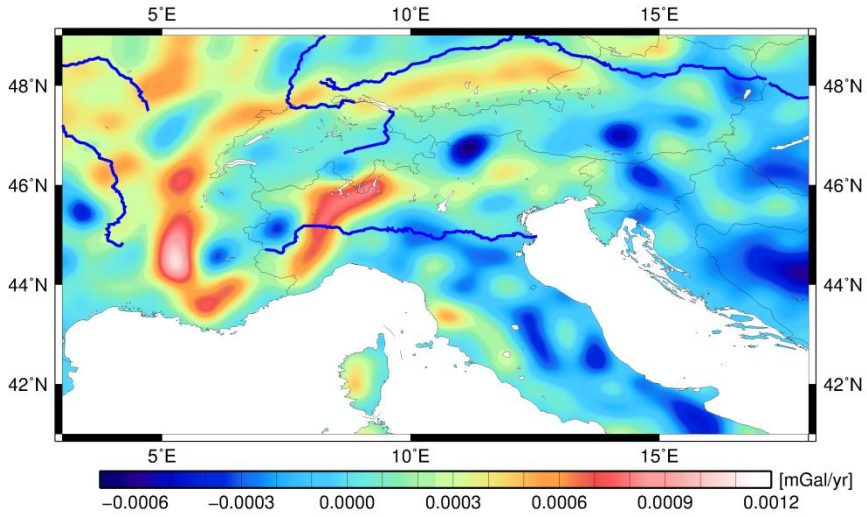

b

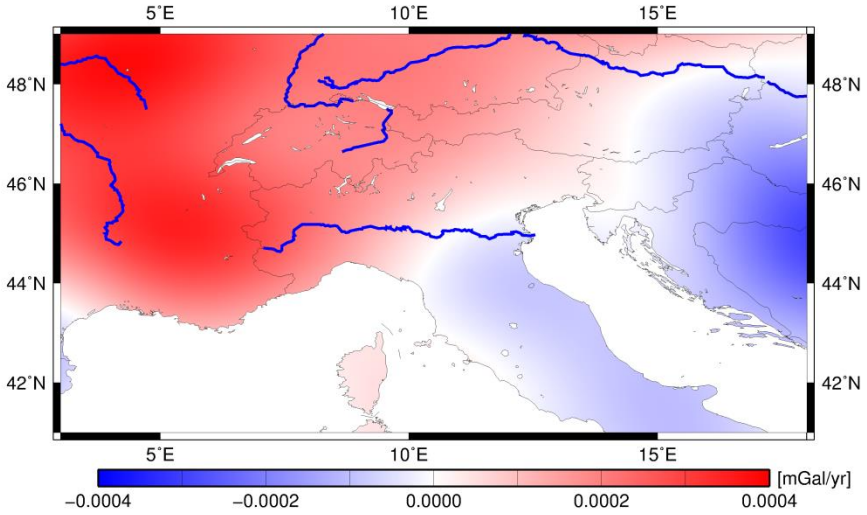

c

Fig.9 (a) GLDAS soil moisture linear change rate (2003-2013); **(b)** the corresponding gravity change rate up to degree/order 720; **(c)** the corresponding gravity changes up to degree/order 100.

For illustration, we select a north-south (A-B) and east-west (C-D) profile (see Fig.10) to display the different signals. Profile A-B cuts the Apennines, the Po basin and the Alps, centered on longitude 11°, and profile C-D cuts the Massif Central, the Alps and the Pannonian basin, centered on latitude 46°. From profile A-B (see

Fig.10a) we find that the ongoing uplift measured by **GPS** is contributing to increase the existing topography, and has maximum uplift rates 0.5° south of the maximum topography. The flat basin area is in strong subsidence. The observed gravity change rate over the same period has the same order of magnitude, but not the same pattern, since gravity increases over the Po basin and decreases over the Alps. An important outcome of our work is that the tectonic uplift/subsidence contributes to a signal that is in the order of magnitude of the observations. It can therefore not be dismissed as negligible. The fact that it does not match the observations implies that the tectonic correction is necessary in order to correctly evaluate the remaining contributors to the observed gravity change signal. The correspondence between tectonic and observed gravity rate does not improve in the profile C-D (see Fig.10b): in fact it shows that moving from the Massif Central to the Alps the observed signal is independent of surface uplift. Only close to the Pannonian basin the topography subsidence matches the observed negative change rate. From the above analysis we can see that the resolution of the present gravity satellite missions is such that tectonic gravity effects must be considered in order to catch the correct hydrological signal. Since the vertical ground motion rates are widely monitored by **GPS**, the tectonic correction can be made in many areas of the globe. A bonus for future satellite missions, with much higher spatial and temporal resolution, is to allow distinguishing the tectonic signal from the climatic signal.

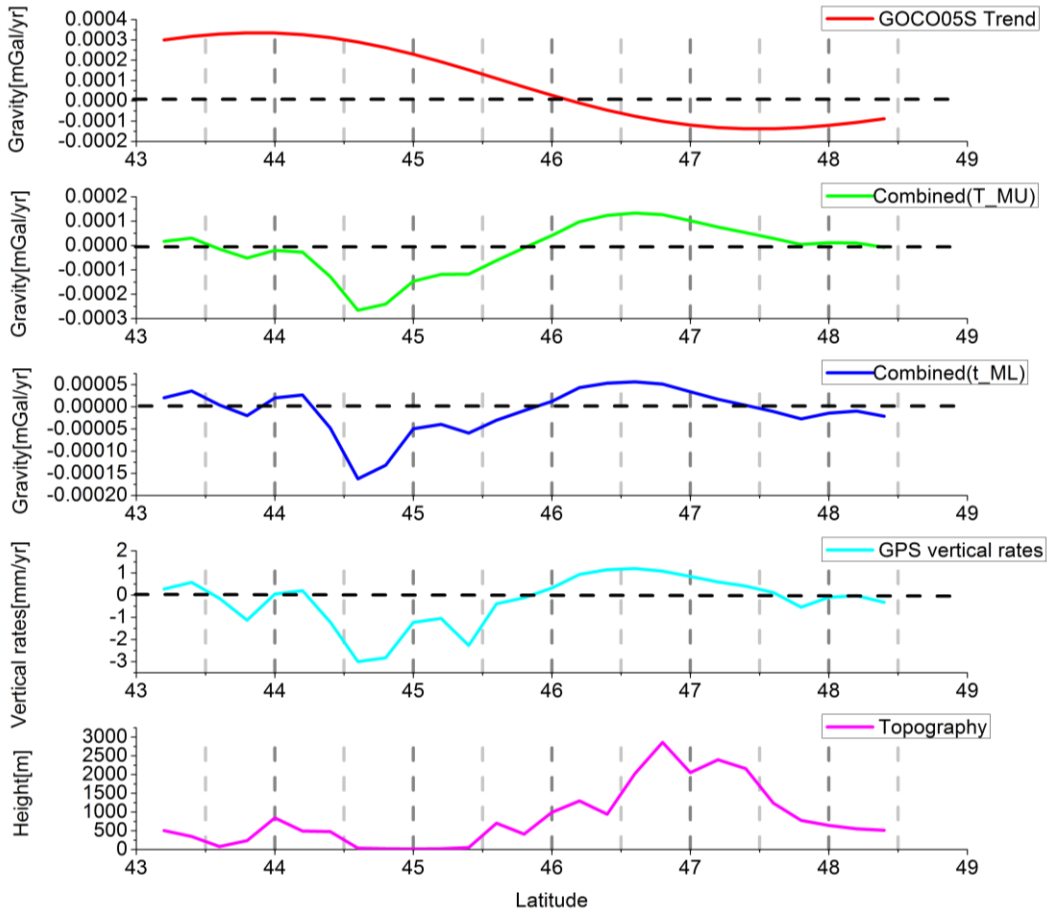

a

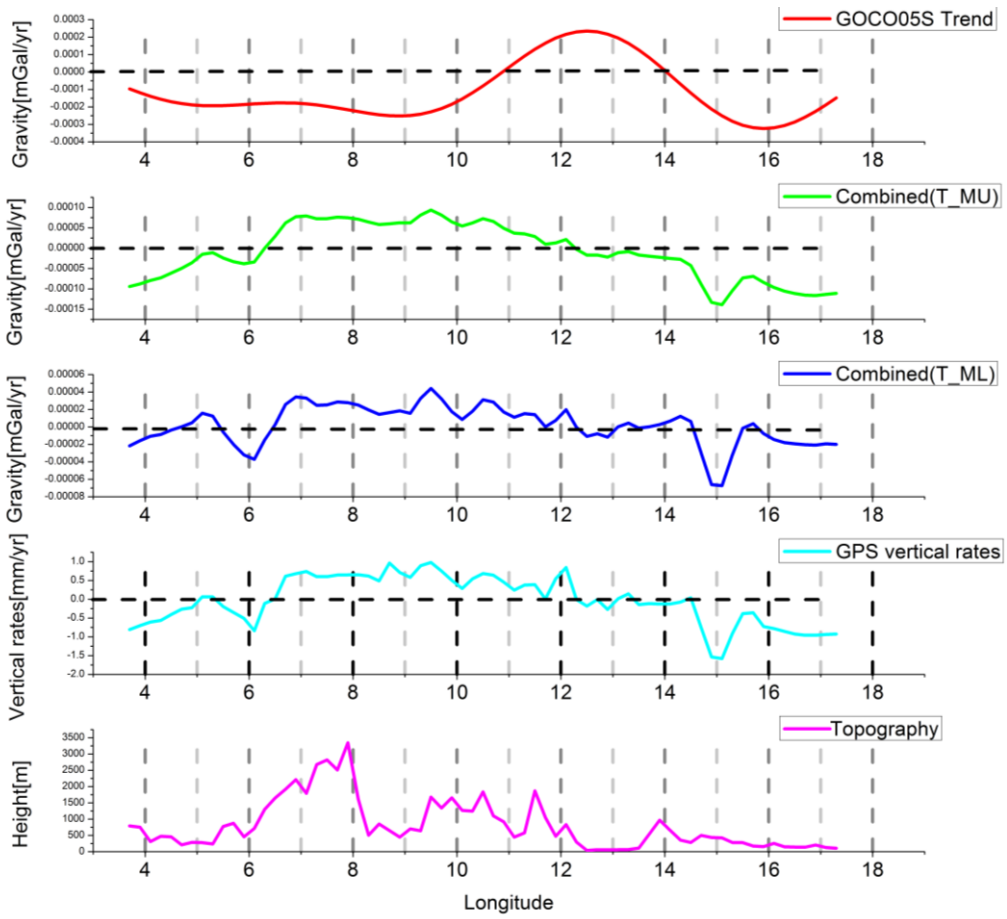

b

Fig.10 (a) A-B profile (GOCO05S Trend stands for observation gravity change, Combined(T_MU) stands for the combined gravity changes of topographic uplift and the corresponding Moho uplift, Combined(T_ML)) stands for the combined gravity changes of topographic uplift and the corresponding Moho lowering, Topography stands the topography along the profile.); **(b)** C-D profile (ibid)

5. Summary and concluding remarks

Two mechanisms are modeled for the expected gravity change rate over the Alpine arc and surrounding areas, based on the vertical surface movement rates from dense **GPS** observations. We computed topographic uplift, associated Moho uplift

considering an unchanged crustal thickness, and Moho lowering due to crustal thickening. The two models predict gravity changes that are at the level of 10^{-3} mGal/yr, with the effect of pure topography uplift being bigger than Moho uplift and a bit bigger and of opposite sign than the Moho lowering due to isostatic crustal thickening. From the above analysis we conclude that tectonic effects cannot be neglected when studying gravity changes over orogens, since it contributes to about 20% in amplitude of the observed signal. Ground water level changes contribute to a gravity signal of up to 20 10^{-3} mGal/yr in the region affected by the greatest water drawdown, converting piezometric water rise to underground water level change. This value is an absolute upper limit, as it is probably smaller by a factor 10 to 100 due to porosity, that is the mass change would be reduced if only the percentage of void spaces would be substituted by water. The GLDAS-1 Noah model of soil moisture is consistent with the pattern shown from the piezometers, where available. The GLDAS-1 derived rates are up to 1 10^{-3} mGal/yr. The two models topography/Moho models and the hydrologic models do not explain the observed gravity change over the Alpine arc, which has a pattern uncorrelated with the topographic uplift and partly correlated with the hydrology. The observed rate likely contains another signal that masks the tectonic signal and is not present in the hydrologic observations. If the goal of a future study would be to distinguish between one or the other geodynamic uplift first the remainder signal has to be reduced. In the Pannonian basin the observations and the model both predict a matching negative gravity change rate.

The complete understanding of the various mechanisms that drive topography

uplift involves broad disciplines such as modeling the crustal stress and deformation, rheology of the crust and lithosphere, and accumulation of seismic energy. The precise and high resolution observed gravity change gives constrains on the possible geodynamic models, because the deep density changes must fit the gravity change rates. Our work shows that the distinction between crustal uplift and crustal thickening requires the recovery of the field at the level of $0.1\ 10^{-3}$ mGal/year, with a resolution of 100km. This field requirement is achievable with a satellite mission of the improved GOCE type, but with a life-span expectance of at least 6 years, in order to robustly retrieve the gravity rates. The yearly and seasonal signal enters the observations, and can be corrected by statistical analysis starting with a time interval of about 6 cycles. The work presented in this study sets the requirements for the next generation of gravity satellite missions when one goal is to model the geodynamic processes of the orogen at deep crustal level.

Acknowledgements

We thank Annette Eicker for helpful discussions, and Giovanni Martinelli for helpful discussions and retrieval of hydrologic data. We thank the Environmental Protection Agencies of Piedmont, Lombardy, Veneto and Emilia Romagna and the Friuli Venezia Giulia Region for piezometric data supply during the S3-DPC-INGV 2012-2015 project. Robert Tenzer is thanked for critical review of the paper.

References

Alvarez, O., Nacif, S., Gimenez, M., Folguera, A., Braitenberg, C., 2014. GOCE derived vertical gravity gradient delineates great earthquake rupture zones along the Chilean margin. Tectonophysics, 622, 198-215

Alvarez, O., Gimenez, M. E., Martinez, M. P., Klinger, F. L., Braitenberg, C., 2015a. New insights into the Andean crustal structure between 32 and 34 S from GOCE satellite gravity data and EGM2008 model. Geological Society, London, Special Publications, 399(1), 183-202.

Alvarez, O., Nacif, S., Spagnotto, S., Folguera, A., Gimenez, M., Chlieh, M., Braitenberg, C., 2015b. Gradients from GOCE reveal gravity changes before Pisagua Mw= 8.2 and Iquique Mw= 7.7 large megathrust earthquakes. Journal of South American Earth Sciences, 64, 273-287.

Altamimi, Z., X. Collilieux, and L. Métivier (2011), ITRF2008: an improved solution of the international terrestrial reference frame, J Geodesy, 85(8), 457–473, doi:10.1007/s00190-011-0444-4.

Amante, C., Eakins, B. W., 2009. ETOPO1 1 arc-minute global relief model: procedures, data sources and analysis (p. 19). Colorado: US Department of Commerce, National Oceanic and Atmospheric Administration, National Environmental Satellite, Data, and Information Service, National Geophysical Data Center, Marine Geology and Geophysics Division.

Bock, H., Jäggi, A., Ulrich Meyer, U., Visser, P., van den Ijssel, J., van Helleputte, T., Heinye, M., Hugentobler, U., 2011. GPS-derived orbits for the GOCE satellite, Journal of Geodesy, 85, 807–818, DOI 10.1007/s00190-011-0484-9.

Bomfim, E. P., Braitenberg, C., Molina, E. C., 2013. Mutual evaluation of global gravity models (EGM2008 and GOCE) and terrestrial data in Amazon Basin, Brazil. Geophysical Journal International, 195(2), 870-882.

Braitenberg, C., Pettenati, F., Zadro, M., 1997. Spectral and classical methods in the evaluation of Moho undulations from gravity data: the NE Italian Alps and isostasy. Journal of Geodynamics, 23(1), 5-22.

Braitenberg, C., 2014. A grip on Geological Units with GOCE In: U. Marti (ed.), Gravity, Geoid and Height Systems, International Association of Geodesy Symposia, 141, 309-317, Springer, doi:10.1007/978-3-319-10837-7_39.

Braitenberg, C., 2015. Exploration of tectonic structures with GOCE in Africa and across-continents. International Journal of Applied Earth Observation and Geoformation, 35, 88-95.

Braitenberg, C., Shum, C. K., 2017. Geodynamic implications of temporal gravity changes over Tibetan Plateau. Italian Journal of Geosciences, 136(1), 39-49.

Champagnac, J. D., Molnar, P., Anderson, R. S., Sue, C., Delacou, B., 2007. Quaternary erosion-induced isostatic rebound in the western Alps. Geology, 35(3), 195-198.

Champagnac, J. D., Schlunegger, F., Norton, K., von Blanckenburg, F., Abbühl, L. M., Schwab, M., 2009. Erosion-driven uplift of the modern Central Alps. Tectonophysics, 474(1), 236-249.

Chao, B. F., Gross, R. S., 1987. Changes in the Earth's rotation and low-degree gravitational field induced by earthquakes. Geophysical Journal International, 91(3), 569-596.

Chéry, J., Genti, M., Vernant, P., 2016. Ice cap melting and low-viscosity crustal root explain the narrow geodetic uplift of the Western Alps. Geophysical Research Letters, 43(7), 3193-3200.

Cloetingh, S. Burov, E., 2011. Lithospheric folding and sedimentary basin evolution: a review and analysis of formation mechanisms. Basin Research 23, 257-290. doi: 10.1111/j.1365-2117.2010.00490.x.

Cloetingh, S., Ziegler, P.E., 2009. Tectonic models for the evolution of sedimentary basins, in: Watts, A.B. (editor) Treatise on Geophysics, Crust and Lithosphere Dynamics, 485-611. Elsevier, Amsterdam.

Dewey, J. F., Pitman, W. C., Ryan, W. B., Bonnin, J., 1973. Plate tectonics and the evolution of the Alpine system. Geological Society of America Bulletin, 84(10), 3137-3180.

Dong, D., Fang, P., Bock, Y., Webb, F., Prawirodirdjo, L., Kedar, S., Jamaso, P., 2006. Spatio-temporal filtering using PCA and KLE approaches for regional GPS network analysis, J. Geophys. Res. 111, No. B03405, doi:10.1029/2005JB003806, 2006.

Ebbing, J., 2004. The crustal structure of the Eastern Alps from a combination of 3D gravity modelling and isostatic investigations. Tectonophysics, 380(1), 89-104.

Faccenna, C., Becker, T. W., Miller, M. S., Serpelloni, E., Willett, S. D., 2014. Isostasy, dynamic topography, and the elevation of the Apennines of Italy, Earth and Planetary Science Letters, 407(C), 163–174, doi:10.1016/j.epsl.2014.09.027.

Fox, M., Herman, F., Kissling, E., Willett, S. D., 2015. Rapid exhumation in the Western Alps driven by slab detachment and glacial erosion. Geology, 43(5), 379-382.

Floberghagen, R., Fehringer, M., Lamarre, D., Muzi, D., Frommknecht, B., Steiger, C., Piñeiro, J., da Costa, A., 2011. Mission design, operation and exploitation of the gravity field and steady-state ocean circulation explorer mission. Journal of Geodesy, 85, 749-758.

Gerrard, J., 1990. Mountain environments: an examination of the physical geography of mountains. MIT Press, 326 pp., ISBN-10: 0262071282.

Hinze, W. J., 2003. Bouguer reduction density, why 2.67?. Geophysics, 68(5), 1559-1560.

Laske, G., Masters, G., Ma, Z., Pasyanos, M., 2013. Update on CRUST1.0-A 1-degree global model of Earth's crust. Geophys. Res. Abstracts, Vol. 15, 20132658abstrEGU.

Levandowski, W., Jones, C. H., Shen, W., Ritzwoller, M. H., Schulte-Pelkum, V., 2014. Origins of topography in the western US: Mapping crustal and upper mantle density variations using a uniform seismic velocity model. Journal of Geophysical Research: Solid Earth, 119(3), 2375-2396.

Li, H., Fang, J., Braitenberg, C., 2017. Lithosphere density structure beneath the eastern margin of the Tibetian Plateau and its surrounding areas derived from GOCE gradients data. Geodesy and Geodynamics, 8, 3, 147-154, doi:10.1016/j.geog.2017.02.007,

Lippitsch, R., Kissling, E., Ansorge, J., 2003. Upper mantle structure beneath the Alpine orogen from high-resolution teleseismic tomography. Journal of Geophysical Research: Solid Earth, 108(B8).

Lyon-Caen, H., Molnar, P., 1989. Constraints on the deep structure and dynamic processes beneath the Alps and adjacent regions from an analysis of gravity anomalies. Geophysical Journal International, 99(1), 19-32.

Mayer-Guerr, T., GOCO team, 2015. The combined satellite gravity field model GOCO05s. Geophysical Research Abstracts, Vol. 17, EGU2015-12364, EGU General Assembly 2015.

Martinelli, G., Chahoud, A., Dadomo, A., Fava, A., 2014. Isotopic features of Emilia-Romagna region (North Italy) groundwaters: Environmental and climatological implications, Journal of Hydrology, 519, 1928–1938.

Molnar, P., England, P., 1990. Temperatures, heat flux, and frictional stress near major thrust faults. Journal of Geophysical Research: Solid Earth, 95(B4), 4833-4856.

Nocquet, J.-M., Sue, C., Walpersdorf, A., Tran, T., Lenôtre, N., Vernant, P., Cushing, M., Jouanne, F., Masson, F., Baize, S., Chéry, J., van der Beek, P.A., 2016. Present-day uplift of the western Alps. Scientific Reports, 6, 28404, doi: 10.1038/srep28404

Pail, R., Bingham, R., Braitenberg, C., Dobslaw, H., Eicker, A., Guntner, A., Horwath, M., Ivins, E., Longuevergne, L., Panet, I., Wouters, B., IUGG Expert Panel, 2015a. Science and User Needs for Observing Global Mass Transport to Understand Global Change and to Benefit Society. Surveys in Geophysics, 36(6), 743-772, doi:10.1007/s10712-015-9348-9.

Pail, R., Bingham, R., Braitenberg, C., Eicker, A., Horwath, M., Ivins, E., Longuevergne, L., Panet, I., Wouters, B., Balsamo, G., Becker, M., Bertrand, D., Bolten, J. D., Boy, J.-P., van den Broeke, M., Cazenave, A., Chambers, D., van Dam, T., Diament, M., van Dijk, A., Dobslaw, H., Doll, P., Ebbing, J., Famiglietti, J., Feng, W., Forsberg, R., van de Giesen, N., Greff, M., Guntner, A., Guo, J.-Y., Han, S.-C., Hanna, E., Heki, K., Hete'nyi, Gy., Jayne, S., Jiang, W., Jin, S., Kaser, G., King, M., Kohl, A., Kunstmann, H., Kusche, J., Lay, T., Locher, A., Lutchke, S., Marcos, M., van der Meijde, M., Mikhailov, V., Ohlwein, Ch., Pollitz, F., Pokhrel, Y., Ponte, R., Rodell, M., Rolstad-Denby, C., Save, H., Scanlon, B., Seneviratne, S., Seyler, F., Shepherd, A., Song, T., Spakman, W., Shum, C. K., Steffen, H., Sun, W., Tang, Q., Tiwari, V., Velicogna, I., Wahr, J., van der Wal, W., Wang, L., Xie, H., Yeh, H.-C., Yeh, P., Zaitchik, B., Zlotnicki, V., 2015b. Observing Mass Transport to Understand Global Change and and to benefit Society: Science and User Needs. Deutsche Geodätische Kommission der Bayerischen Akademie der Wissenschaften, Reihe B, Angewandte Geodäsie, Heft Nr. 320, 1-124, ISSN 0065-5317, ISBN: 978-3-7696-8599-2.

Pail, R., Bruinsma, S., Migliaccio, F., Förste, C., Goiginger, H., Schuh, W.D., Höck, E., Reguzzoni, M., Brockmann, J.M., Abrikosov, O., Veicherts, M., Fecher, T., Mayrhofer, R., Krasbutter, I., Sanso, F., Tscherning, C.C., 2011. First GOCE gravity field models derived by three different approaches, Journal of Geodesy 85, 819– 843, doi: 10.1007/s00190- 011-0467-x.

Pfiffner, O. A., 2014. Geology of the Alps. John Wiley & Sons.

Rebischung, P., Griffiths, J., Ray, J., Schmid, R., Collilieux, X., Garayt, B., 2011. IGS08: the IGS realization of ITRF2008, GPS Solut, 16, 483-494, doi:10.1007/s10291-011-0248-2.

Rodell, M., Houser, P. R., Jambor, U. E. A., Gottschalck, J., Mitchell, K., Meng, C.-J., Arsenault, K., Cosgrove, B., Radakovich, J., Bosilovich, M., Entin, J.K., Walker, J.P., Lohmann, D., Toll, D., 2004. The global land data assimilation system. Bulletin of the American Meteorological Society, 85, , 381-394.

Serpelloni, E., Faccenna, C., Spada, G., Dong, D., Williams, S. D., 2013. Vertical GPS ground motion rates in the Euro-Mediterranean region: New evidence of velocity gradients at different spatial scales along the Nubia-Eurasia plate boundary. Journal of Geophysical Research: Solid Earth, 118, , 6003-6024.

Serpelloni, E., Vannucci, G., Anderlini, L., Bennett, R. A., 2016. Kinematics, seismotectonics and seismic potential of the eastern sector of the European Alps from GPS and seismic deformation data, Tectonophysics, 688, 157–181, doi:10.1016/j.tecto.2016.09.026.

Shin, Y. H., Shum, C. K., Braitenberg, C., Lee, S. M., Na, S. H., Choi, K. S., Hsu, H., Park, Z.S., Lim, M., 2015. Moho topography, ranges and folds of Tibet by analysis of global gravity models and GOCE data. Scientific Reports, 5, 11681.

Singer, J., Diehl, T., Husen, S., Kissling, E., Duretz, T., 2014. Alpine lithosphere slab rollback causing lower crustal seismicity in northern foreland. Earth and Planetary Science Letters, 397, 42-56.

Smith, W. H. F, Wessel, P., 1990. Gridding with continuous curvature splines in tension, Geophysics, 55, 293-305.

Tapley, B. D., Bettadpur, S., Ries, J. C., Thompson, P. F., Watkins, M. M., 2004a. GRACE measurements of mass variability in the Earth system. Science, 305(5683), 503-505.

Tapley, B. D., Bettadpur, S., Watkins, M., Reigber, C., 2004b. The gravity recovery and climate experiment: Mission overview and early results. Geophysical Research Letters, 31(9).

Uieda, L., Barbosa, V. C., Braitenberg, C., 2016. Tesseroids: Forward-modeling gravitational fields in spherical coordinates. Geophysics, 81(5), F41-F48, doi:10.1190/geo2015-0204.1.

Vernant, P., Hivert, F., Chery, J., Steer, P., Cattin, R., Rigo, A., 2013. Erosion-induced isostatic rebound triggers extension in low convergent mountain ranges. Geology, 41(4), 467-470.

Wahr, J., Molenaar, M., Bryan, F., 1998. Time variability of the Earth's gravity field: Hydrological and oceanic effects and their possible detection using GRACE. Journal of Geophysical Research: Solid Earth, 103(B12), 30205-30229.

Wu, X., Collilieux, X., Altamimi, Z., Vermeersen, B., Gross, R. S., Fukumori, I.,2011. Accuracy of the international terrestrial reference frame origin and earth expansion. Geophys. Res. Lett., 38, L13304, https://doi.org/10.1029/2011GL047450.

Highlights:

- The GOCE gravity field revolutionized the details in geologic regional structures that can and were identified.
- Here we seek to interpret for the first time the most recent GOCE gravity field, obtained optimizing the entire GOCE acquisition series, and integrating it with the field from satellite GRACE.
- The new time variable field has higher resolution than that from GRACE alone and we interpret it over the entire Alpine range.
- We find that the resolution of the field is such, that the orogen building mechanism can be distinguished, whether a pure uplift or a crustal thickening. The Alpine uplift contributes to 20% of the observed GOCE field, which displays a variation that cannot be attributed to neither hydrology nor tectonic uplift, and requires further investigation.